Lab on a Chip

Miniaturisation for chemistry, physics, biology, materials science and bioengineering

www.rsc.org/loc

Volume 13 | Number 14 | 21 July 2013 | Pages 2663–2850

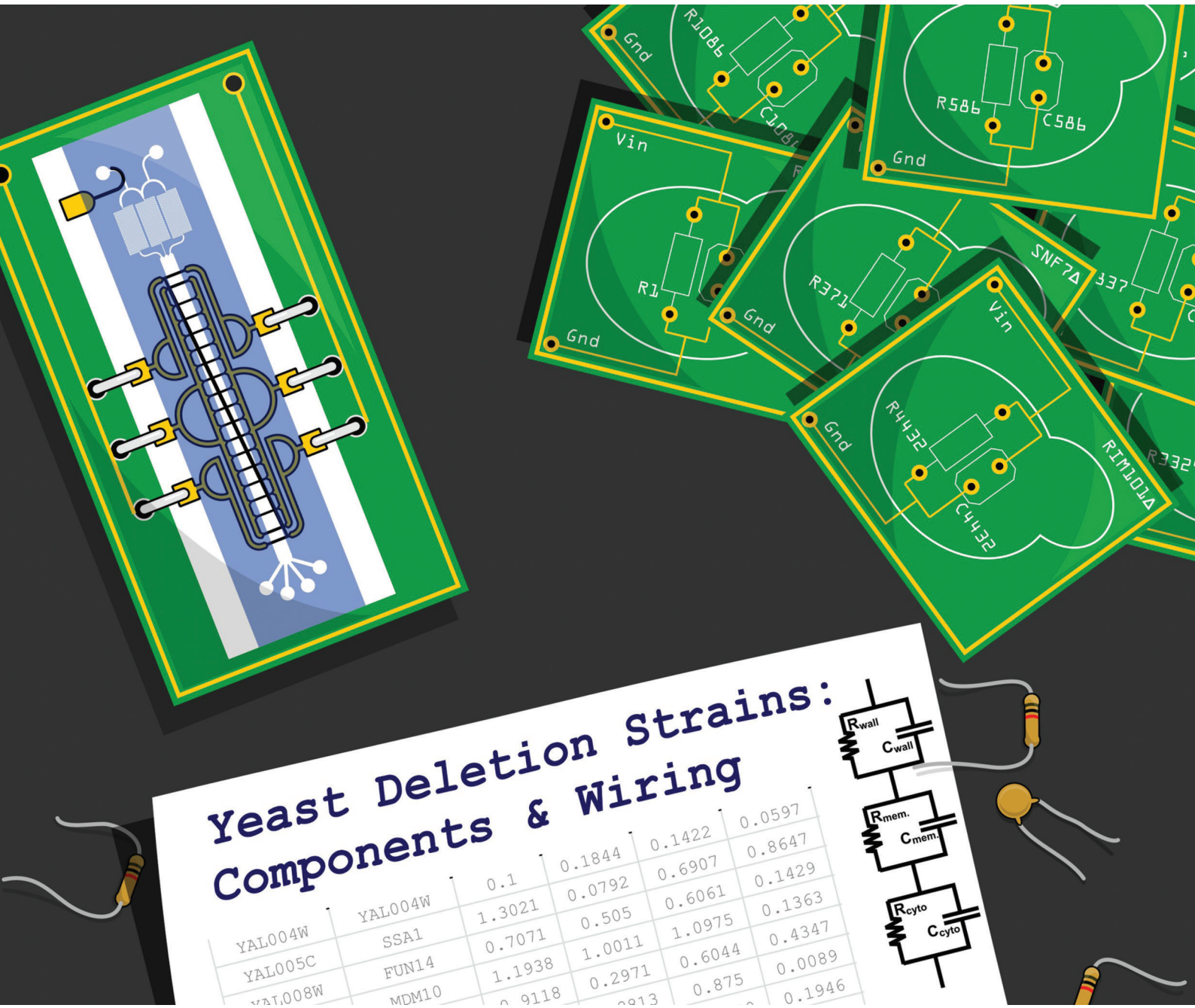

ISSN 1473-0197

RSC Publishing

PAPER

Joel Voldman *et al.*

Microfluidic genome-wide profiling of intrinsic electrical properties in *Saccharomyces cerevisiae*

Lab on a Chip

RSC Publishing

PAPER

View Article Online
View Journal | View Issue

Microfluidic genome-wide profiling of intrinsic electrical properties in *Saccharomyces cerevisiae*†

Cite this: *Lab Chip*, 2013, **13**, 2754

Michael D. Vahey,‡[a] Laia Quiros Pesudo,[b] J. Peter Svensson,[c] Leona D. Samson[b] and Joel Voldman*[a]

Methods to analyze the intrinsic physical properties of cells – for example, size, density, rigidity, or electrical properties – are an active area of interest in the microfluidics community. Although the physical properties of cells are determined at a fundamental level by gene expression, the relationship between the two remains exceptionally complex and poorly characterized, limiting the adoption of intrinsic separation technologies. To improve our current understanding of how a cell's genotype maps to a measurable physical characteristic and quantitatively investigate the potential of using these characteristics as biomarkers, we have developed a novel screen that combines microfluidic cell sorting with high-throughput sequencing and the haploid yeast deletion library to identify genes whose functions modulate one such characteristic – intrinsic electrical properties. Using this screen, we are able to establish a high-content electrical profile of the haploid yeast gene deletion strains. We find that individual genetic deletions can appreciably alter the electrical properties of cells, affecting ~10% of the 4432 gene deletion strains screened. Additionally, we find that gene deletions affecting electrical properties in specific ways (*i.e.* increasing or decreasing effective conductivity at higher or lower electric field frequencies) are strongly associated with an enriched subset of fundamental biological processes that can be traced to specific pathways and complexes. The screening approach demonstrated here and the attendant results are immediately applicable to the intrinsic separations community.

Received 4th February 2013,
Accepted 25th April 2013

DOI: 10.1039/c3lc50162k

www.rsc.org/loc

Published on 25 April 2013. Downloaded on 15/02/2015 00:38:33.

Introduction

Analysis and sorting of cell subpopulations is widespread throughout biology and medicine. Discriminating cell subpopulations requires biological markers that are specific and sensitive to the phenotype of interest. The development and discovery of new biological markers is thus a major driving force in both biotechnology, medicine and fundamental cell biology. Biomarkers come in a variety of forms at the single-cell level, such as the expression of individual or ensembles of genes or proteins,[1–3] functional characteristics such as enhanced sensitivity or tolerance to environmental conditions,[4] and direct inspection of a cell's physical characteristics, commonly known as intrinsic markers.[5–8] The usefulness of a biomarker is fundamentally tied to its specificity and sensitivity (*i.e.* how closely correlated it is to one particular phenotype and not to others), as well as its versatility (*i.e.* how easily it can be measured). As a result, before a new biomarker can effectively be employed, these central questions related to its utility must be answered.

Among these different categories of biomarkers, the physical characteristics of cells are particularly appealing candidates for high-throughput applications because their intrinsic nature makes them measurable on intact cells, with little or no sample processing required. As a result of their non-invasive nature, essentially all physical properties of cells (*e.g.*, mechanical, electrical, optical) have been explored as biological markers, often using microfluidic systems.[9–15] A common thread among all of these physical characteristics is that they offer a complex, integrated view of cellular physiology not simply arising from the sum of the molecules that make up the cell, but rather depending on the complex organization and interactions of these molecules. As a result, predicting the physical properties of a cell requires not only a detailed knowledge of the cell's components, but also an understanding of how these components are arranged spatially and temporally throughout the cell. The challenge and complexity inherent in making this type of prediction presents a fundamental obstacle in the systematic development of

[a]*Department of Electrical Engineering and Computer Science, Massachusetts Institute of Technology, Cambridge, MA 02139, USA. E-mail: voldman@mit.edu; Fax: +1 617.258.5846; Tel: +1 617.253.2094*
[b]*Biological Engineering Department, Center for Environmental Health Sciences, Biology Department, Koch Institute for Integrative Cancer Research, Massachusetts Institute of Technology, Cambridge, MA 02139, USA*
[c]*Department of Biosciences and Nutrition, Karolinska Institutet, 14183 Huddinge, Sweden*

† Electronic supplementary information (ESI) available. See DOI: 10.1039/c3lc50162k

‡ Currently at the Department of Bioengineering, University of California Berkeley, Berkeley, CA 94720, USA.

This journal is © The Royal Society of Chemistry 2013

Published on 25 April 2013. Downloaded on 15/02/2015 00:38:33.

physical characteristics as biomarkers and is a primary bottleneck in the adoption of microfluidic technologies to discriminate cells based on those characteristics.

Although this type of bottom-up prediction of physical properties is currently intractable, an alternate top-down approach is to work backwards from a set of physical characteristics to establish the underlying genetic basis that gave rise to those characteristics. This mapping of genotype to complex physical phenotype can provide comprehensive guidelines for using physical properties as biomarkers in a systematic way. Facile methods to map the connection between genotype and physical properties would have wide applicability across intrinsic cell analysis methods, helping to determine which genotypes are most amenable to analysis with particular intrinsic properties.

To demonstrate the feasibility of this approach for a specific class of physical characteristics – the intrinsic electrical properties of a cell – we developed a screen to determine genes whose functions modulate electrical conductivity and permittivity at the single-cell level. The screen leverages three recently developed tools: the genetically barcoded haploid yeast deletion library;[16] high-throughput sequencing-based techniques for quantifying strain abundance;[17] and microfluidic technology for high-specificity cell sorting based on differences in the intrinsic electrical properties of individual cells.[18] By sorting the deletion collection into fractions with different electrical characteristics and counting the relative abundance of each strain within the different fractions, we are able to generate for the first time a genome-wide mapping between genotype and electrical phenotype. This mapping reveals that electrical properties are largely independent of (and thus complimentary to) other phenotypic data including fitness and morphology, and allows us to identify specific processes and pathways whose perturbations can be detected through changes in electrical properties. While these results are directly applicable to the wide range of methods used to analyze and sort cells according to their electrical properties, they also serve to demonstrate the feasibility of performing whole-genome screens based on intrinsic properties, a methodology that can be translated to other devices that sort cells based upon other physical properties.

Results

To separate cells according to their electrical properties, we employed a microfluidic dielectrophoretic separation method called isodielectric separation (IDS)[18,19] (Fig. 1a). Cells subjected to an external electric field become polarized in a manner dependent upon the electrical conductivity and permittivity of the cell relative to that of the suspending medium.[20] If there is a gradient in the properties of the suspending medium, cells can therefore be localized to the regions where their electrical polarization vanishes. IDS is analogous to isoelectric focusing, but is sensitive to polarization rather than charge. This dielectrophoretic equilibrium (the isodielectric point, to extend the analogy to isoelectric focusing) is specifically related to the electrical conductivity and permittivity of a cell in a frequency-dependent manner; at lower frequencies, the equilibrium position is sensitive to the external cell layers, whereas at higher frequencies, the sensitivity shifts to the cell interior. Additionally, the separation is first-order insensitive to other intrinsic properties like size, density, compressibility, *etc*.

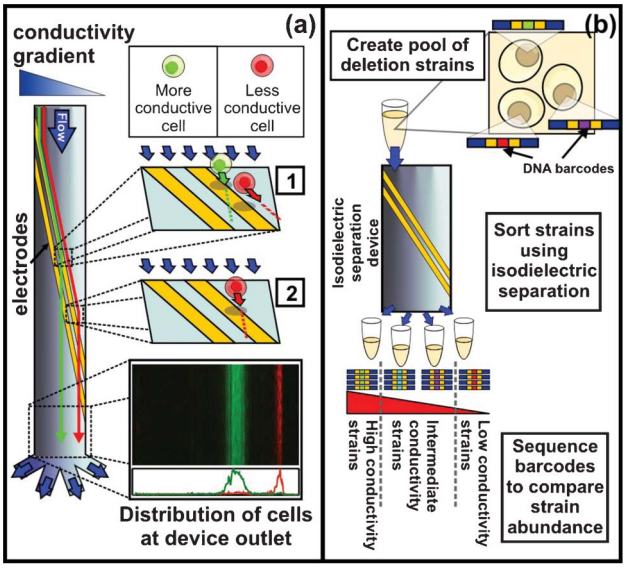

Fig. 1 Screening the yeast deletion strains using isodielectric separation. (a) Overview of device operation: cells enter the device in liquid with a relatively high electrical conductivity (left side of gradient indicated by blue shading) and are retained by the dielectrophoretic force generated at the electrodes. As the cells are deflected across a transverse liquid conductivity gradient to lower conductivities, the force acting on cells with different conductivities decreases at a different rate; first, more conductive cells (green) pass through the barrier (1), followed by less conductive cells (red) further along the channel width (2), giving rise at the outlet to different spatial distributions for populations of cells with different electrical properties. (b) Work flow for the screen: starting from a pool of the deletion strains, we use isodielectric separation to sort cells into different outlets, corresponding to higher and lower conductivities. Sequencing barcodes from each sorted fraction quantifies the abundance of each strain and identifies gene deletions that change the effective conductivity of a cell.

To determine how (and if) single gene deletions could affect the physical properties of cells, we applied IDS to screen the yeast haploid gene deletion library, comparing strain enrichments in fractions of the pooled deletion library sorted to different conductivities and read out through deep barcode sequencing[17] (Fig. 1b). In this fashion we identified genes whose deletion changes the electrical properties of the host cell.

Determining operating conditions for the separation

Before proceeding to perform the screen, we first sought to determine appropriate operating conditions for the separation. One requirement for the screen is high throughput, which will assure sufficient sampling of each deletion strain in the population of cells we collect. In order to determine the

Published on 25 April 2013. Downloaded on 15/02/2015 00:38:33.

throughput our screen would require, we used a simple statistical model to determine the number of cells we would need to collect (= N) to sample each of M equally represented mutant strains a minimum of K times (see ESI† Discussion for details):

$$N \approx M\left[K + \log(M) + \sqrt{2K\log(M)}\right] \quad (1)$$

In order to determine N, we chose an appropriate value for K by requiring that it be large enough that the frequency of each strain in the collected samples is an accurate representation of the actual frequency, f. Given that we collect K cells of a particular strain from a single outlet, the probability distribution for the actual frequency of these cells (*i.e.* the frequency we would observe if we collected infinitely many cells) under the given conditions is:

$$p(f) = N\binom{N}{K}(f)^K(1-f)^{N-K} \approx \frac{N(fN)^K}{K!}\exp\{-fN\} \quad (2)$$

The first and second moments of this distribution are $\langle f\rangle = (K+1)/N$ and $\langle f^2\rangle = (K+1)(K+2)/N^2$, so that the uncertainty in f decreases relative to the mean as $\sim K^{-1/2}$. Therefore, to assure that the sensitivity of the screen is not limited by the number of cells we collect, a reasonable level of redundancy is to require $K \sim 400$, corresponding to a detection limit of $\sim$5% (other unrelated factors may increase this limit). Since the haploid deletion library is comprised of $M \sim 5000$ strains, this requires collecting about 2.5 million cells from each of the four outlets.

Adapting a model we previously developed,[18] the operating flow rate for IDS (= Q) is constrained by device geometry and operating conditions according to:

$$Q_{\max} \approx \frac{\varepsilon_m V_0^2 aL}{250\mu H}|K| \quad (3)$$

Here, ε_m and μ denote the permittivity and viscosity of the suspending medium, V_0 is the amplitude of the applied voltage, a is the cell radius ($\sim$3 μm for yeast), L and H are the length and depth of the device, respectively, and K is the threshold polarizability. In order to maximize the sensitivity of the separation, we want the threshold polarizability to be low; for a device with dimensions of 2 mm wide × 20 μm deep × 30 mm long and an operating voltage of 10 V, selecting $|K|$ = 0.05 will allow us to operate at a flow rate of $\sim$4 μl min^{-1} while maintaining $\sim$90% insensitivity to variations in cell size.[18] Injecting cells into the device at a density of $\sim 2 \times 10^7$ cells ml^{-1} under these conditions allows us to reach our target of $\sim 10^7$ cells in two to three hours of continuous operation.

Distribution of deletion strain conductivities at lower and higher electric field frequencies

Using these operating conditions, we performed pooled screens at electric field frequencies of 300 kHz (to probe the properties of the cell envelope) and 10 MHz (to probe the properties of the cell interior). From these, we determined the mean and variance in conductivity for each strain, as a measure of how electrically distinguishable they are. The average conductivity per strain was distributed around 0.031 ± 0.001 Ω^{-1} m^{-1} at 300 kHz, and 0.23 ± 0.008 Ω^{-1} m^{-1} at 10 MHz (Fig. 2), with an asymmetric bias towards strains with increased conductivity at the lower frequency (skewness ∼ 1.2 for the central part of the distribution), and a bias towards decreased conductivity at the high frequency (skewness ∼ −1.3). In contrast to the narrow distribution in average conductivity across strains, the standard deviation in conductivity within individual strains is approximately five- to seven-fold larger (±0.007 Ω^{-1} m^{-1} at 300 kHz and ±0.043 Ω^{-1} m^{-1} at 10 MHz, see ESI† Methods and ESI† Datasets S1 and S2). This implies that genetically distinct cells with measurably different average conductivities will typically have overlapping distributions; electrical phenotypes (and potentially other physical properties) have limited specificity.

To identify strains whose electrical properties substantially differ on average from the composite pool, we defined a log ratio describing the abundance of each strain sorted into higher *vs.* lower conductivity fractions (Fig. 3a and b, see Methods and ESI† Datasets S1 and S2). From this log ratio, we identified 419 strains ($\sim$10% of the 4432 strains represented in the screen) with enrichment >2 s.d. from the mean under at least one of the screening conditions. Pairwise comparisons between a subset of enriched deletion strains and the parental wildtype strain suggest a false positive rate of $\sim$10% (ESI† Methods and ESI† Fig. S1), demonstrating that electrical properties are indeed widely sensitive to genotype, and that gene deletions can both increase and decrease effective conductivity, depending upon the gene. Additionally, we observed low correlation between the electrical properties of strains at lower *versus* higher frequencies (Pearson's $r \sim 0.10$ *versus* $\sim$0.48 for independent experiments under identical conditions), consistent with the different sensitivities of the screening conditions to the cell envelope (at 300 kHz) and cell interior (at 10 MHz). This low correlation suggests that

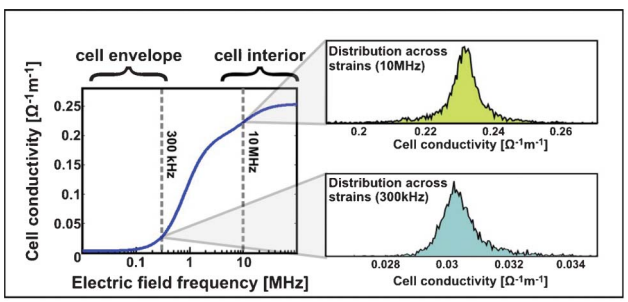

Fig. 2 Distribution of effective conductivity across the yeast deletion strains at lower and higher electric field frequencies. The plot to the left shows a model for the effective conductivity of a single cell as a function of frequency; lower frequencies probe the cell envelope while higher frequencies probe the cell interior. At higher electric field frequencies (10 MHz, upper right), the cell conductivity is determined primarily by the cell cytoplasm and intracellular organelles and has an average value of $\sim$0.23 ± 0.008 Ω^{-1} m^{-1}; at lower frequencies (300 kHz, lower right), the comparatively insulating cell envelope becomes dominant, and the average conductivity across all strains is $\sim$0.031 ± 0.001 Ω^{-1} m^{-1}.

 This journal is © The Royal Society of Chemistry 2013

Published on 25 April 2013. Downloaded on 15/02/2015 00:38:33.

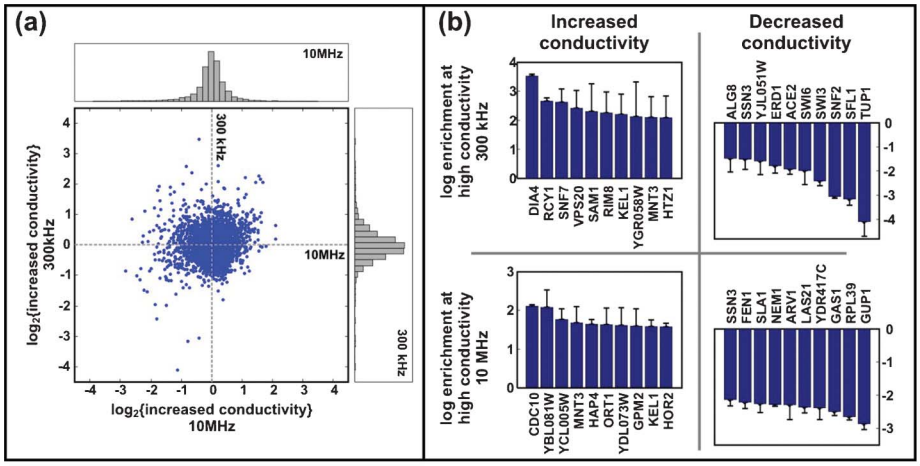

Fig. 3 Different genes influence electrical properties as measured at different electric field frequencies (300 kHz and 10 MHz). (a) Log ratios for increased/decreased conductivity at 300 kHz (vertical axis) and 10 MHz (horizontal axis) for each strain included in the screen, Correlation between genes that alter electrical properties at lower and higher frequencies is low (Pearson's $r \sim 0.10$), consistent with the different sensitivities to the cell envelope and interior under these respective conditions. (b) Strains showing the greatest increase or decrease in conductivities at each field condition. Error bars show one standard deviation in the log ratio of electrical enrichment for the given electric field frequency.

mutations affecting electrical properties exhibit reasonable specificity to the inner or outer compartments of the cell. These results show that single genetic changes can appreciably alter the electrical properties of cells (which we find to be the case in about 10% of the deletions we have screened), and that screening under multiple conditions allows us to increase the specificity of the experiment, by refining subpopulations of cells according to their properties over a range of frequencies.

Fitness & morphology

One of the benefits of the yeast haploid gene deletion library is that it has been extensively phenotyped. This allowed us to correlate changes in electrical properties to other phenotypic changes due to deletions. This analysis can provide insight into the mechanism underlying how genetic deletions can affect electrical properties. For example, to determine if electrically distinct phenotypes were correlated with fitness defects (*i.e.*, growth under various stresses), we compared our electrical profiling data to existing fitness profiles of the deletion strains.[4,16,21] Comparing fitness profiles, we find an overlap of approximately 30% between strains showing increased or decreased effective conductivities and those exhibiting fitness defects in rich medium (Fig. 4a and ESI† Methods). Under altered environmental conditions,[4] electrical properties correlate with different sensitivities; matching these changes in electrical properties with their associated fitness defects provides a connection between the structural and the functional changes that accompany a gene deletion. For example, strains with increased cell envelope conductivity have a high incidence of ionic sensitivity (>10-fold higher

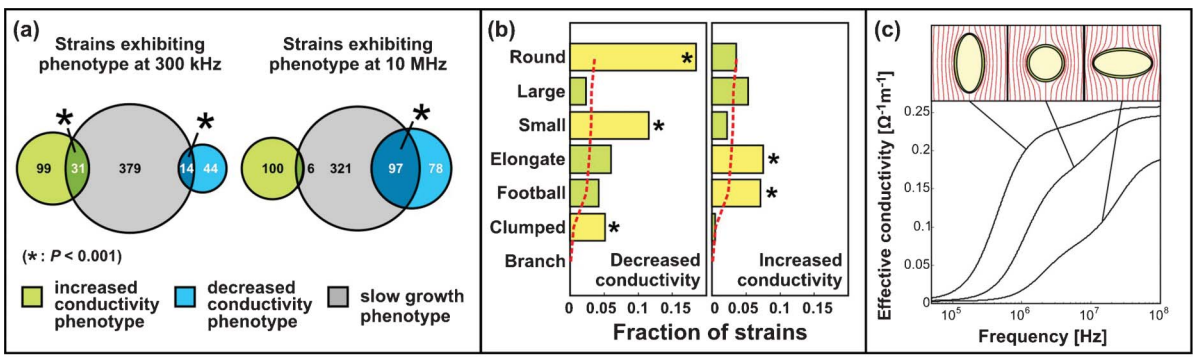

Fig. 4 Comparison of electrical phenotypes with growth and morphology phenotypes. (a) Correlation between strains exhibiting altered electrical properties and those exhibiting fitness defects in YPD. Overall, ~30% of strains with altered electrical properties exhibit a fitness defect in YPD, with the largest overlap occurring for strains with decreased cytoplasmic conductivity. A ''*'' indicates overlap between phenotypes that is significantly enriched over expectation ($P < 0.001$). (b) Strains with decreased effective conductivity are significantly ($P < 0.01$) enriched for ''round'', ''small'', and ''clumped'' morphologies, whereas strains with increased effective conductivity are enriched for ''elongate'' and ''football'' morphologies. (c) Prediction for how the frequency-dependent conductivity of a cell will depend on the cell's shape and orientation in an electric field. Elongated strains aligned to the external field exhibit increased effective conductivity relative to round strains and strains aligned perpendicular to the external field.

Published on 25 April 2013. Downloaded on 15/02/2015 00:38:33.

than expectation; $P < 10^{-5}$, see ESI† Methods) while strains with decreased cytoplasmic conductivity are enriched for sensitivity to nutritional limitations (>5-fold higher representation than across the genome, $P < 10^{-3}$, see ESI† Methods).

We next compared our results with morphological categorization of the deletion strains;[16] because electrical properties are tightly and mechanistically linked to cell shape, we could determine 1) whether changes in shape would alter the electrical properties as predicted from electromagnetic theory, and 2) whether all electrically distinct strains arose merely due to changes in shape. The relationship between the morphology of a cell and its electrical properties can be modeled by approximating cells as prolate ellipsoids sheathed by confocal ellipsoids representing the cell membrane and wall.[22] For a prolate ellipsoidal cell comprised of three confocal layers with major axis a_i, minor axis c_i, and eccentricity $e_i^2 = 1 - c_i^2/a_i^2$, (where i = 1,2,3 for cytoplasm, membrane, and cell wall, respectively), the polarizability can be determined using the depolarization factors, ($\ell_i^{\perp}$ and $\ell_i^{||}$) to reduce the layered ellipsoid to an equivalent, homogeneous ellipsoid. Specifically, the effective permittivity of a particle aligned parallel to the electric field can be determined by iteratively using (for each of n cell layers, where n increases in the external direction):

$$\underline{\varepsilon}'_n = \underline{\varepsilon}_n \left[\frac{\underline{\varepsilon}_n + (\underline{\varepsilon}'_{n-1} - \underline{\varepsilon}_n)\ell^{||}_{n-1} + (a_{n-1}c^2_{n-1}/a_n c^2_n)(\underline{\varepsilon}'_{n-1} - \underline{\varepsilon}_n)(1-\ell^{||}_n)}{\underline{\varepsilon}_n + (\underline{\varepsilon}'_{n-1} - \underline{\varepsilon}_n)\ell^{||}_{n-1} - (a_{n-1}c^2_{n-1}/a_n c^2_n)(\underline{\varepsilon}'_{n-1} - \underline{\varepsilon}_n)\ell^{||}_n} \right] \quad (4)$$

From this, the polarizability can be calculated using:

$$\underline{K} = \left[\frac{\underline{\varepsilon}'_{\mathrm{p}} - \underline{\varepsilon}_{\mathrm{m}}}{3(\underline{\varepsilon}_{\mathrm{m}} + (\underline{\varepsilon}'_{\mathrm{p}} - \underline{\varepsilon}_{\mathrm{m}})\ell^{||}_{\mathrm{p}})} \right] \quad (5)$$

Here, the complex permittivity is given by $\varepsilon_i = \varepsilon_i + \sigma_i/i\omega$ and the depolarization factors are given by:

$$\ell_i^{||} = \frac{c_i^2}{2a_i^2 e_i^3}\left[\log\left\{\frac{1+e_i}{1-e_i}\right\} - 2e_i\right] \quad ; \quad \ell_i^{||} + 2\ell_i^{\perp} = 1 \quad (6)$$

Eqn (5) and (6) can be modified for a particle perpendicular to the field by replacing $\ell_i^{||}$ with $\ell_i^{\perp}$ everywhere. Note that, in assuming that the cell layers are confocal, the cell wall and cell membrane thickness vary over the surface of the cell. For two confocal ellipsoids, the distance between their surfaces along the major and minor axes are $\Delta_a = (a^2 + \xi^2)^{1/2} - a$ and $\Delta_c = (c^2 + \xi^2)^{1/2} - c$, respectively, where surfaces of constant ξ describe confocal ellipsoids. If we choose to define Δ_c as the wall/membrane thickness, the thickness along the major axis will be approximately smaller by a factor of c/a; accordingly, this approximation may become inaccurate for strongly elongated ellipsoids. Nonetheless, the salient feature of these equations is that, as a cell becomes increasingly elongated, $\ell_i^{||} \rightarrow 0$ and $\ell_i^{\perp} \rightarrow$ ½. This amounts to an increase in the effective conductivity of a cell aligned with the field, and a decrease for a particle perpendicular to the applied field (Fig. 4c). Although cells will initially have arbitrary orientation, application of a strong field will exert a torque that tends to align their major axis in the direction of the field (although under some special conditions, they may align perpendicular to the field,[22] this is not the case here). This alignment, although not complete in the presence of fluid flow exerting an additional torque on elongated cells, can be directly observed in our experiments. The result is that the effective conductivity of elongated cells is predicted to increase, while the effective conductivity of more rounded cells will decrease.

We did observe a significant enrichment ($P < 10^{-6}$) of strains classified as having elongated morphologies at higher conductivity, and more rounded, small, or clumped morphologies at lower conductivities (Fig. 4b). These enrichments are consistent with the theoretical predictions described above and illustrated in Fig. 4c. However, our data show that morphological changes are neither necessary nor sufficient to change the electrical properties of a cell; the majority of morphologically distinct strains exhibit wildtype electrical properties, and for each category of electrically distinct strains, between 50 and 70% are identified as having wildtype morphology (ESI† Fig. S2). Thus, our results are consistent with electromagnetic theory; more interestingly, however, they point to a substantial set of mutations that alter electrical properties through changes that are more subtle than those associated with visibly different morphology.

Protein localization & abundance

We next examined whether changes in the electrical properties of the cell envelope or intracellular space would be attributable to the deletion of proteins localizing to these compartments, or whether the connection between gene deletion and electrical change would be more complex. For instance, one might reasonably anticipate that changes in the envelope electrical properties would be caused by genes whose protein products localized to the envelope. However, by comparing our data to protein localization data,[23] we found that a significantly enriched fraction of genes whose deletion changes cell envelope conductivity code for proteins that localize to the cytoplasm and nucleus (Fig. 5a; ESI† Table S1). The predominance of intracellular proteins among those that affect the electrical properties of the cell envelope suggests that downstream functional consequences of a protein's absence determine electrical differences, rather than the direct physical consequences of the protein's absence. This hypothesis is supported by the low correlation between protein abundance[24] and electrical phenotype ($r = -0.095$; see ESI† Methods and ESI† Fig. S3), as well as the high rate at which the deletion of regulatory genes alter electrical properties. For example, we find that strains with decreased cell envelope conductivity are significantly enriched for GO biological process terms ''RNA metabolic processes'' and ''transcription'' ($P \sim 10^{-5}$ and $P \sim 10^{-4}$, respectively; Fig. 5b, left).

For strains with altered intracellular conductivity, we similarly observe no correlation with protein abundance data ($r = 0.026$; see ESI† Methods and ESI† Fig. S3). However, among the decreased conductivity subset of these strains, we do observe enrichment in those lacking intracellular proteins: specifically, those localizing to the mitochondrion, nucleolus, and vacuolar membrane (Fig. 5a). The biological processes associated with these organelles suggests a connection

 This journal is © The Royal Society of Chemistry 2013

Published on 25 April 2013. Downloaded on 15/02/2015 00:38:33.

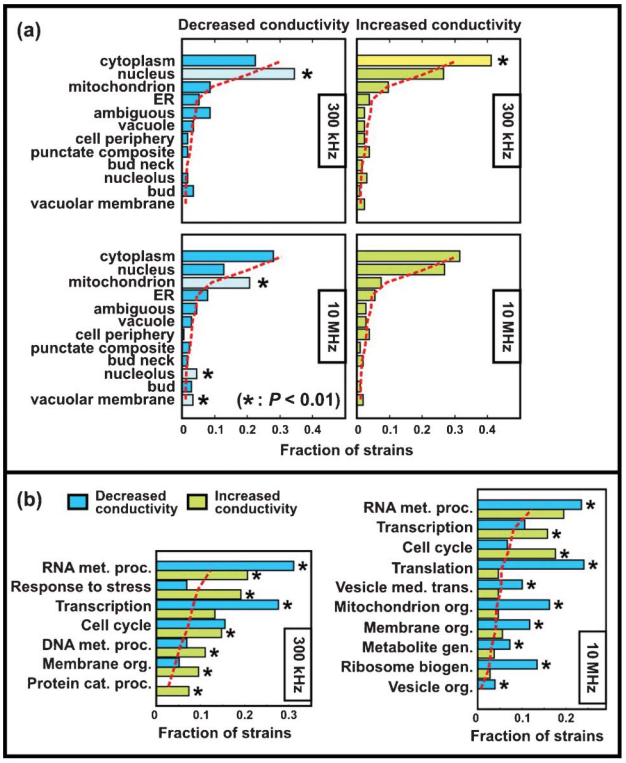

Fig. 5 Comparisons between electrical properties and other phenotypic data. (a) Localization of proteins whose deletion confers an increase or decrease in conductivity. The red dotted line represents the frequency of occurrence for each localization category in the overall gene deletion library. (b) Gene Ontology biological process terms strongly associated with increased/decreased conductivity of the cell envelope (top, 300 kHz) and cytoplasm (bottom, 10 MHz). A ''*'' denotes significantly enriched categories ($P < 0.001$).

between biosynthetic processes and cytoplasmic conductivity; genes whose deletion leads to decreased intracellular conductivity have significantly enriched GO biological process terms including translation ($P \sim 10^{-12}$), ribosome biogenesis ($P \sim 10^{-11}$), and mitochondrion organization ($P < 10^{-10}$) (Fig. 5b, right; see ESI† Table S2 and ESI† Dataset S3). Similar to our findings for genes associated with increased cell envelope conductivity, the association between increased intracellular conductivity and the cell's central metabolic machinery provides an argument for approaching intrinsic separations on a more comprehensive scale. Essentially, linkages between a genotype and phenotype are not generally superficial, and thus it is not possible in the majority of cases to *a priori* determine which biological phenotypes are likely to be amenable to measurement or detection using a given intrinsic property. As a result of this more subtle link between genotype and intrinsic phenotype, it is critical that new approaches to empirically and systematically map the applicability of intrinsic separations be developed. Indeed it is probably because the connection between genotype and physical phenotype occurs through a complicated genetic regulatory network that the deletion of a single gene is sufficient to alter the overall electrical properties of a cell.

Genetic interactions

To test the hypothesis that genes affecting electrical properties preferentially act upstream in regulatory networks, we compared our electrical profile with datasets for genetic interactions.[25] In this analysis, we differentiate between positive genetic interactions (which indicate a functional dependence between two genes) and negative interactions (which indicate a functional redundancy).[26] Since the number of positive genetic interactions that a gene exhibits indicates its position within the overall network hierarchy, we used genetic interaction data to determine if genes associated with changes in electrical properties were enriched for these interactions, and thus tended to act as regulatory hubs. To perform this analysis, we identify genes associated with a specific electrical phenotype and determine (1) the number of interactions associated with these genes in total and (2) the number of interactions that are internal to this sub-network (see ESI† Methods and ESI† Table S3). We find that genes associated with either increased cell envelope conductivity or decreased cytoplasmic conductivity are enriched approximately twofold over expectation in number of total interactions. In addition, genes associated with these electrical phenotypes form sub-networks that are more highly interconnected than would be predicted from the connectivity of the overall genetic landscape; for cells with increased cell envelope conductivity, connectivity is enriched $>4\times$ over expectation ($P \sim 10^{-8}$), and for genes associated with decreased intracellular conductivity, the enrichment is $>3\times$ over expectation ($P \sim 10^{-6}$). This enrichment is consistent with comparisons to protein-protein interaction data[27] (ESI† Table S3), and supports the conclusion that changes in electrical properties arise from perturbations to functional networks within the cell, rather than through the direct influence of individual genes.

Pathways and complexes

To identify specific pathways and complexes whose disruption is associated with altered electrical properties, we focused on the sub-networks of positive genetic interactions associated with either decreased cell envelope conductivity or increased cytoplasmic conductivity. This led us to investigate the Rim101 pathway and its relationship to the ESCRT machinery,[28,29] and the role of each in determining the electrical properties of a cell. The Rim101 pathway, activated by the proteolytic cleavage of the zinc-finger transcription factor Rim101p, is involved in alkaline pH response, sensing of lipid asymmetry, ion homeostasis, cell wall maintenance, sporulation, and glucose repression.[30–33] In our screen, we find that strains lacking Rim101 or upstream genes involved in its activation (including ESCRT proteins) exhibit increased cell envelope conductivity relative to wildtype cells (Fig. 6a, left), while strains lacking ESCRT proteins exhibit decreased cytoplasmic conductivity (Fig. 6a, right); this results in a pleiotropic electrical phenotype for strains lacking genes involved in both pathways (*e.g.* SNF7, VPS36, STP22, among others; Fig. 6b). We generated strains lacking both RIM101 (or its activator, RIM8) and NRG1, a downstream target for repression, and found that they exhibit restored wildtype electrical properties (Fig. 6c). This is in contrast to strains we generated lacking both RIM101 (or

Published on 25 April 2013. Downloaded on 15/02/2015 00:38:33.

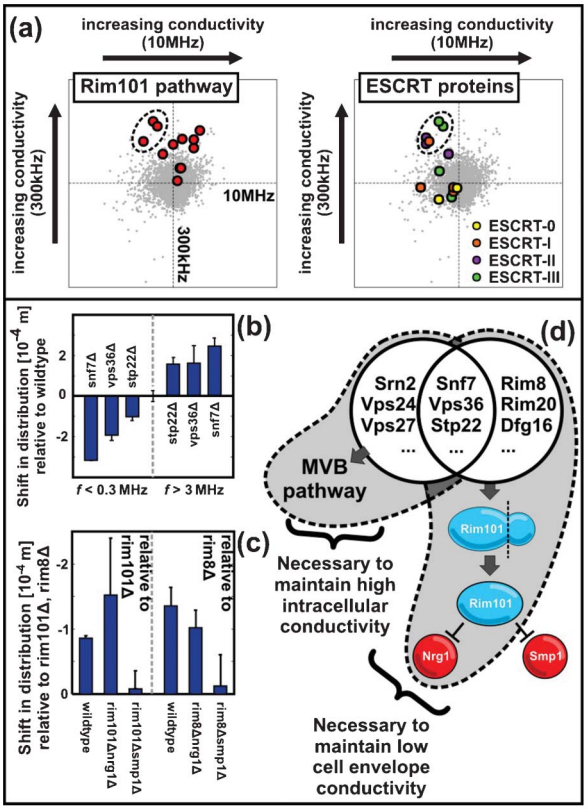

Fig. 6 Pathways and complexes associated with changes in electrical properties. (a) Plots of strain conductivities at 300 kHz and 10 MHz highlighting genes associated with the Rim101 pathway (left) and endosomal trafficking (right). Proteins associated with the Rim101 pathway (overlayed in red on the distribution of electrical log ratios) include a subset of ESCRT proteins whose deletion increases the cell envelope conductivity (top half of the 300 kHz axis), but decreases the cytoplasmic conductivity (left half of the 10 MHz axis). (b) ESCRT proteins that participate in the Rim101 pathway (snf7, vps36 and stp22) exhibit opposite electrical phenotypes at higher and lower electric field frequencies, as determined through pairwise comparisons with wildtype cells. Error bars show one standard deviation about the mean. (c) Deleting NRG1 from strains lacking either RIM101 or RIM8 restores wildtype electrical properties, whereas deleting SMP1 does not, as determined by measuring their shift in conductivity relative to Rim101 or Rim8 deletion strains. (d) A model for how electrical pleiotropy arises from disruptions to overlapping gene networks. Deleting genes participating in the RIM101 pathway (RIM101, RIM8, RIM20, DFG16 and others, including a subset of ESCRT genes) increases the conductivity of the cell envelope. This change can be suppressed by the additional deletion of NRG1, but not SMP1. Independently, disruption of the MVB pathway (including the deletion of ESCRT genes) decreases the cytoplasmic conductivity, so that strains lacking genes associated with both Rim101 and ESCRTs exhibit pleiotropic electrical phenotype.

RIM8) and SMP1 (a second downstream target for repression involved in sporulation), demonstrating that the alteration of electrical properties in mutants deficient in the Rim101 pathway arises downstream of NRG1, possibly through RSB1 (a regulator of lipid asymmetry) or ENA1 (a sodium efflux pump). Although the molecular mechanism through which effective conductivity is altered in this case remains to be determined, this combination of traditional genetic approaches with electrical phenotyping demonstrates a means of linking the intrinsic physical properties of a cell to specific genes within a complex regulatory network (Fig. 6d).

Discussion

In creating an electrical profile of the haploid yeast deletion collection, we demonstrate an approach to map genotype to an intrinsic physical property, and identify connections between changes to biological function and electrical properties. This screen demonstrates that the deletion of a single gene is sufficient to substantially alter the electrical properties of a cell for ~10% of non-essential genes; however, it is interesting to note that these genes tend to participate in processes that affect the physiology of a cell at a global level, through their involvement in transcription, translation, and protein trafficking. This belies the naïve expectation that, for example, genes with a direct involvement in ion transport or cell wall biosynthesis would comprise the predominant results of the screen due to their direct involvement in processes with clear implications for the conductivity and permittivity of the cell. Also contrary to our initial expectations, we find that although the morphology of a cell does contribute to its electrical properties as predicted from electrostatics theory, the overlap is less than 50%. These results demonstrate the difficulty inherent in predicting changes in electrical properties based on the function of a single gene or from other phenotypic data. Although this places a mechanistic description of electrical phenotype beyond the scope of this work, it reinforces the concept that intrinsic physical properties encode more subtle information than simply a component list for a cell; the organization of these components and their interactions with each other is also of critical importance.

If electrical properties are to be used as biomarkers, an important consideration is how specifically they correspond to a particular biological state. We find that individual gene deletions typically alter the average electrical properties of a strain to a lesser extent than the inherent variability within a strain and thus have modest specificity, but that these average changes in conductivity exhibit significant correlations with specific pathways and biological processes, demonstrating that electrical properties may be applicable as markers for a wide variety of biological states, especially those associated with metabolic defects. This potential, combined with the throughput and relative ease with which electrical properties of cells can be characterized, establishes electrical screening as a versatile method.

An important challenge in the future will be to complement this versatility by increasing the specificity of electrical properties, or any other intrinsic physical property, as well. Our results show that screening cells under different conditions (lower or higher electric field frequencies) provides information that is largely orthogonal; the low correlation between gene deletions that alter electrical properties at lower and higher electric field frequencies demonstrates that screening cells under multiple conditions can substantially

 This journal is © The Royal Society of Chemistry 2013

Published on 25 April 2013. Downloaded on 15/02/2015 00:38:33.

enhance the specificity of a screen. Additionally, increasing the number of outlets across which the cells are fractionated (or varying their spatial distribution across these outlets) will help to resolve increasingly subtle differences in electrical properties between strains.

While here we use this screening methodology to investigate the genetic basis for electrical differences between cells, this methodology could be extended to a variety of other physical characteristics. The abundance of high-throughput label-free techniques for sorting cells based on intrinsic physical properties could be applied in the same manner, creating a foundation for assessing biological state with high specificity through combinatorial measurements of complementary physical characteristics. Critical to interpretation of the results is the use of sorting methods that are specific to the property of interest; methods that are sensitive to a combination of properties (*e.g.*, size and density) would make it more difficult to determine whether a particular genetic change influenced one or the other (or both) properties.

Conclusions

We report the first genome-wide mapping between genotype and an intrinsic property, in this case electrical phenotype. By combining a microfluidic device that is specific to electrical properties with the yeast deletion library and next-generation sequencing, we demonstrate a methodology applicable for investigating the connection between genotype and other physical properties as well. We find that single gene deletions can indeed appreciably alter electrical properties, and that they do so in non-trivial ways. Further, by taking advantage of the rich genetics of yeast, we are able to begin to investigate the pathways involved in these changes. Although there remains a significant gap between our current understanding of the genetics underlying intrinsic physical properties – and in particular the underlying basis of variations within genetically homogeneous populations – the work presented here demonstrates the feasibility of addressing this challenge through new screening technologies.

Experimental

Operation of the isodielectric separation device

The design and fabrication of the isodielectric separation device has previously been described.[18,19] To perform separations, the device electrodes are driven by a function generator at either 300 kHz (to probe the cell envelope) or 10 MHz (to probe the cell interior). For separations at a frequency of 300 kHz, the conductivity range spans from 0.065 S m^{-1} to 0.01 S m^{-1}; at 10 MHz, the range is from 0.35 S m^{-1} to 0.12 S m^{-1}. Under these conditions, the distribution of cells is approximately symmetric about the center of the channel, with a width comparable to that of the channel. Since this results in a slight surplus of cells in the two central outlets relative to the two outer ones, we constrain the throughput for the screen based on the number of cells collected in the two outermost outlets to avoid sampling artifacts. The electrical conductivity of the medium is adjusted through the addition of phosphate buffered saline, in addition to 0.5% bovine serum albumin to minimize non-specific adhesion of cells to the surface of the device during separations.

Deletion pool construction, cell culture, and sample preparation for sorting

Pools of the yeast haploid deletion collection were prepared as described previously.[34] Prior to performing separations, we cultured the deletion pools at 30 °C and 250 rpm in an incubator shaker using media containing 10 g l^{-1} yeast extract, 20 g l^{-1} peptone, 20 g l^{-1} dextrose, and 100 μg ml^{-1} G418 for ~4 generations to a concentration of $\sim 3 \times 10^8$ cells ml^{-1}. For separations, cells were washed and re-suspended in the separation medium at a concentration of $\sim 5 \times 10^7$ cells ml^{-1}.

Creation of double deletion mutants

We created two double deletion strains as described previously[35] to test the rescue of electrical phenotype in cells lacking the Rim101 transcription factor or a gene involved in its activation. We mated both rim101Δ and rim8Δ cells (*MAT*α, KanMX marker) separately with nrg1Δ and smp1Δ cells (*MAT*a, URA3 marker) and selected for diploids on SD-URA medium with 100 μg ml^{-1} G418. After sporulation of diploid cells, we selected for *MAT*a haploids containing both URA3 and KanMX selectable markers using Magic Medium[35] lacking uracil and supplemented with 100 μg ml^{-1} G418.

Sequencing

Samples were sequenced on a Solexa Genome Analyzer 2.0, generating single ends reads of 35 nucleotides. The first four bases comprise the multiplexing code used to assign each read to an experiment and a sample (five total for each experiment: one of four sorted fractions or the original pool). The next set of bases identify whether the read corresponds to an uptag or downtag barcode, and the final 14 bases (13 for uptags) provides sufficient information to uniquely identify the barcode.[17] Custom Matlab scripts parse sequencing reads to tabulate the number of perfect barcode reads for each strain in each sample, and for each experiment.

Analysis of sequencing results

The tabulated counts for each strain are normalized to a frequency for each sample so that we can compare frequencies in the different sorted fractions to the frequencies in the original (unsorted) pool. These frequencies are calculated separately for uptags and downtags, as well as for each independent experiment (*i.e.* each screen has two independent replicates, so that there are four separate frequency vectors for each sample in each screen). To eliminate spurious hits arising from poorly represented strains, we add a baseline value equal to one tenth the sample mean (= 1/10 *M*, for *M* strains) to each vector of frequencies; this is equivalent to adding 10–20 pseudocounts to the unnormalized vector of counts. Based on these adjusted frequencies, we calculate enrichment as the (strain-by-strain) ratio of each sorted sample to the unsorted pool: f_1/f_0, f_2/f_0, f_3/f_0, f_4/f_0, where 'f_i'

denotes the strain frequency vectors for the i^{th} outlet, with $i = 1$ representing the highest conductivity and $i = 4$ representing the lowest; the subscript '0' denotes the strain frequency vector of the original pool.

We use the strain frequencies in different sorted fractions to define a log ratio, y, which is positive if a strain exhibits increased effective conductivity and negative for strains exhibiting decreased effective conductivity:

$$y \equiv \log_2\left[\frac{\sqrt{f_1 f_2}}{\sqrt{f_3 f_4}}\right]$$

ESI† Datasets S1 and S2 list y values for each strain detected in the screens at 300 kHz and 10 MHz, respectively.

To determine if a specific phenotype is correlated with increased or decreased effective conductivities, we use the log ratio y to identify strains that are electrically distinct and compare this to other phenotypic data associated with each gene deletion characterized in our screen. Details of this analysis for each of the phenotypic categories described in the Results section are included in ESI† Methods.

Published on 25 April 2013. Downloaded on 15/02/2015 00:38:33.

Acknowledgements

We would like to thank A. Dudley for providing a critical reading of the manuscript. This work was supported by the Singapore-MIT Alliance, NSF IDBR grant DBI-0852654, and NIH grant EB005753.

References

1 J. M. Irish, N. Kotecha and G. P. Nolan, *Nat. Rev. Cancer*, 2006, **6**, 146–155.
2 P. O. Krutzik, J. M. Crane, M. R. Clutter and G. P. Nolan, *Nat. Chem. Biol.*, 2007, **4**, 132–142.
3 T. Brambrink, R. Foreman, G. G. Welstead, C. J. Lengner, M. Wernig, H. Suh and R. Jaenisch, *Cell Stem Cell*, 2008, **2**, 151–159.
4 M. E. Hillenmeyer, E. Fung, J. Wildenhain, S. E. Pierce, S. Hoon, W. Lee, M. Proctor, R. P. St. Onge, M. Tyers, D. Koller, R. B. Altman, R. W. Davis, C. Nislow and G. Giaever, *Science*, 2008, **320**, 362–5.
5 S. E. Cross, Y.-S. Jin, J. Rao and J. K. Gimzewski, *Nat. Nanotechnol.*, 2007, **2**, 780–3.
6 S. Suresh, *Acta Biomater.*, 2007, **3**, 413–38.
7 F. Chowdhury, S. Na, D. Li, Y.-C. Poh, T. S. Tanaka, F. Wang and N. Wang, *Nat. Mater.*, 2009, **9**, 82–8.
8 F. F. Becker, X. B. Wang, Y. Huang, R. Pethig, J. Vykoukal and P. R. Gascoyne, *Proc. Natl. Acad. Sci. U. S. A.*, 1995, **92**, 860–4.
9 S. C. Hur, N. K. Henderson-MacLennan, E. R. B. McCabe and D. Di Carlo, *Lab Chip*, 2011, **11**, 912–920.
10 J. M. Maloney, D. Nikova, F. Lautenschläger, E. Clarke, R. Langer, J. Guck and K. J. Van Vliet, *Biophys. J.*, 2010, **99**, 2479–2487.
11 W. H. Grover, A. K. Bryan, M. Diez-Silvac, S. Suresh, J. M. Higgins and S. R. Manalis, *Proc. Natl. Acad. Sci. U. S. A.*, 2011, **108**, 10992–10999.
12 M. J. Rosenbluth, W. A. Lam and D. A. Fletcher, *Lab Chip*, 2008, **8**, 1062–70.
13 P. Thevoz, J. D. Adams, H. Shea, H. Bruus and H. T. Soh, *Anal. Chem.*, 2010, **82**, 3094–8.
14 R. Pethig, V. Bressler, C. Carswell-Crumpton, Y. Chen, L. Foster-Haje, M. E. García-Ojeda, R. S. Lee, G. M. Lock, M. S. Talary and K. M. Tate, *Electrophoresis*, 2002, **23**, 2057–63.
15 L. A. Flanagan, J. Lu, L. Wang, S. A. Marchenko, N. L. Jeon, A. P. Lee and E. S. Monuki, *Stem Cells*, 2008, **26**, 656–65.
16 G. Giaever, A. M. Chu, L. Ni, C. Connelly, L. Riles, S. Véronneau, S. Dow, A. Lucau-Danila, K. Anderson, B. André, A. P. Arkin, A. Astromoff, M. El Bakkoury, R. Bangham, R. Benito, S. Brachat, S. Campanaro, M. Curtiss, K. Davis, A. Deutschbauer, K.-D. Entian, P. Flaherty, F. Foury, D. J. Garfinkel, M. Gerstein, D. Gotte, U. Güldener, J. H. Hegemann, S. Hempel, Z. Herman, D. F. Jaramillo, D. E. Kelly, S. L. Kelly, P. Kötter, D. LaBonte, D. C. Lamb, N. Lan, H. Liang, H. Liao, L. Liu, C. Luo, M. Lussier, R. Mao, P. Menard, S. L. Ooi, J. L. Revuelta, C. J. Roberts, M. Rose, P. Ross-Macdonald, B. Scherens, G. Schimmack, B. Shafer, D. D. Shoemaker, S. Sookhai-Mahadeo, R. K. Storms, J. N. Strathern, G. Valle, M. Voet, G. Volckaert, C.-Y. Wang, T. R. Ward, J. Wilhelmy, E. A. Winzeler, Y. Yang, G. Yen, E. Youngman, K. Yu, H. Bussey, J. D. Boeke, M. Snyder, P. Philippsen, R. W. Davis and M. Johnston, *Nature*, 2002, **418**, 387–91.
17 A. M. Smith, L. E. Heisler, J. Mellor, F. Kaper, M. J. Thompson, M. Chee, F. P. Roth, G. Giaever and C. Nislow, *Genome Res.*, 2009, **19**, 1836–42.
18 M. D. Vahey and J. Voldman, *Anal. Chem.*, 2008, **80**, 3135–43.
19 M. D. Vahey and J. Voldman, *Anal. Chem.*, 2009, **81**, 2446–55.
20 H. A. Pohl and J. S. Crane, *Biophys. J.*, 1971, **11**, 711–27.
21 A. M. Deutschbauer, D. F. Jaramillo, M. Proctor, J. Kumm, M. E. Hillenmeyer, R. W. Davis, C. Nislow and G. Giaever, *Genetics*, 2005, **169**, 1915–25.
22 T. B. Jones, *Electromechanics of Particles*, Cambridge University Press, New York, 1995.
23 W.-K. Huh, J. V. Falvo, L. C. Gerke, A. S. Carroll, R. W. Howson, J. S. Weissman and E. K. O'Shea, *Nature*, 2003, **425**, 686–691.
24 S. Ghaemmaghami, W.-K. Huh, K. Bower, R. W. Howson, A. Belle, N. Dephoure, E. K. O'Shea and J. S. Weissman, *Nature*, 2003, **425**, 737–741.
25 M. Costanzo, A. Baryshnikova, J. Bellay, Y. Kim, E. D. Spear, C. S. Sevier, H. Ding, J. L. Y. Koh, K. Toufighi, S. Mostafavi, J. Prinz, R. P. St. Onge, B. VanderSluis, T. Makhnevych, F. J. Vizeacoumar, S. Alizadeh, S. Bahr, R. L. Brost, Y. Chen, M. Cokol, R. Deshpande, Z. Li, Z.-Y. Lin, W. Liang, M. Marback, J. Paw, B.-J. San Luis, E. Shuteriqi, A. H. Y. Tong, N. van Dyk, I. M. Wallace, J. A. Whitney, M. T. Weirauch, G. Zhong, H. Zhu, W. A. Houry, M. Brudno, S. Ragibizadeh, B. Papp, C. Pal, F. P. Roth, G. Giaever, C. Nislow, O. G. Troyanskaya, H. Bussey, G. D. Bader, A.-C. Gingras, Q. D. Morris, P. M. Kim, C. A. Kaiser, C.L. Myers, B. J. Andrews and C. Boone, *Science*, 2010, **327**, 425–31.
26 A. Baryshnikova, M. Costanzo, Y. Kim, H. Ding, J. Koh, K. Toufighi, J.-Y. Youn, J. Ou, B.-J. San Luis,

 This journal is © The Royal Society of Chemistry 2013

S. Bandyopadhyay, M. Hibbs, D. Hess, A.-C. Gingras, G. D. Bader, O. G. Troyanskaya, G. W. Brown, B. Andrews, C. Boone and C. L. Myers, *Nat. Methods*, 2010, **7**, 1017–1025.

27 N. J. Krogan, G. Cagney, H. Yu, G. Zhong, X. Guo, A. Ignatchenko, J. Li, S. Pu, N. Datta, A. P. Tikuisis, T. Punna, J. M. Peregrín-Alvarez, M. Shales, X. Zhang, M. Davey, M. D. Robinson, A. Paccanaro, J. E. Bray, A. Sheung, B. Beattie, D. P. Richards, V. Canadien, A. Lalev, F. Mena, P. Wong, A. Starostine, M. M. Canete, J. Vlasblom, S. Wu, C. Orsi, S. R. Collins, S. Chandran, R. Haw, J. J. Rilstone, K. Gandi, N. J. Thompson, G. Musso, P. St Onge, S. Ghanny, M. H. Lam, G. Butland, A. M. Altaf-Ul, S. Kanaya, A. Shilatifard, E. O'Shea, J. S. Weissman, C. J. Ingles, T. R. Hughes, J. Parkinson, M. Gerstein, S. J. Wodak, A. Emili and J. F. Greenblatt, *Nature*, 2006, **440**, 637–643.

28 M. Hayashi, T. Fukuzawa, H. Sorimachi and T. Maeda, *Mol. Cell. Biol.*, 2005, **25**, 9478–9490.

29 J. H. Hurley and P. I. Hanson, *Nat. Rev. Mol. Cell Biol.*, 2010, **11**, 556–566.

30 T. M. Lamb, W. Xu, A. Diamond and A. P. Mitchell, *J. Biol. Chem.*, 2001, **276**, 1850–6.

31 M. Ikeda, A. Kihara, A. Denpoh and Y. Igarashi, *Mol. Biol. Cell*, 2008, **19**, 1922–31.

32 T. M. Lamb and A. P. Mitchell, *Mol. Cell. Biol.*, 2003, **23**, 677–86.

33 W. Xu, F. J. Smith, R. Subaran and A. P. Mitchell, *Mol. Biol. Cell*, 2004, **15**, 5528–37.

34 S. E. Pierce, R. W. Davis, C. Nislow and G. Giaever, *Nat. Protoc.*, 2007, **2**, 2958–2974.

35 X. Pan, D. S. Yuan, D. Xiang, X. Wang, S. Sookhai-Mahadeo, J. S. Bader, P. Hieter, F. Spencer and J. D. Boeke, *Mol. Cell*, 2004, **16**, 487–496.

Published on 25 April 2013. Downloaded on 15/02/2015 00:38:33.